Journal of Hazardous Materials 187 (2011) 562–573

Contents lists available at ScienceDirect

Journal of Hazardous Materials

journal homepage: www.elsevier.com/locate/jhazmat

A comparison of basic dye adsorption onto zeolitic materials synthesized from fly ash

Gülten Atun*, Gül Hisarlı, Ayşe Engin Kurtoğlu, Nihat Ayar

Istanbul University, Faculty of Engineering, Department of Chemistry, 34850 Avcılar, Istanbul, Turkey

ARTICLE INFO

Article history:
Received 15 July 2010
Received in revised form 12 January 2011
Accepted 18 January 2011
Available online 26 January 2011

Keywords:
Fly ash zeolites
Adsorption
Basic dyes
Thionine
Safranine T

ABSTRACT

This investigation reveals the adsorption characteristics of two basic dyes, thionine (TH) and safranine T (ST), onto fly ash (FA) and its three zeolitized products prepared at different hydrothermal conditions. Typical two-step isotherms were observed for TH adsorption onto four adsorbents, whereas the isotherms of the larger ST molecules were S-shaped. The adsorption capacities of the zeolitized fly ash (ZFA) estimated from the first plateau region of the TH isotherms was nearly twice the FA capacity. The capacities increased by up to five times in the second plateau region. The adsorption capacity of FA for ST is equivalent that of TH, whereas the capacities of ZFA are lower than those found for TH. The equilibrium results were well-described by the Freundlich isotherm model. The kinetic data obtained in the temperature range of 298–318 K was analyzed using Paterson's and Nernst Plank's approximations based on the homogeneous surface diffusion model (HSDM). The thermodynamic functions for the transition state were evaluated from the temperature-dependence of the surface diffusion coefficients by applying the Eyring model.

1. Introduction

It has been estimated that coal-based thermal power plants annually generate more than 500 million tons of fly ash (FA) as a byproduct [1]. FA is widely used as an additive in the cement and concrete building industry, and is largely still disposed in landfills [2]. There is an active field of research directed towards developing alternate uses for FA, such as adsorption of water pollutants and preparation of zeolitic materials.

Different varieties of fly ash have different sorption propensities for inorganic and organic pollutants such as cesium [3,4], strontium [4], organic-basic [5–15], organic-acidic [5–7,16] and organic-reactive dyes [17,18]. Because the adsorption capabilities of fly ash for cationic species are relatively low, they can be enhanced by surfactant modification [5,13], heat and acid treatment [8,9] and zeolitization under alkaline hydrothermal conditions [1,2,7,10,12,19–35].

Fly ash is an ideal precursor for the production of zeolites, due to its compositional similarity to volcanic materials with high SiO_2 and Al_2O_3 content. Volcanic ash is converted into zeolites in the environment by the action of alkaline/saline surface and/or groundwater in a slow process that takes hundreds to thousands of years [19]. Some zeolitic materials have also been successfully synthesized from FA by relatively inexpensive and quick hydrothermal conversion processes. The fly ash-based zeolites are capable of absorbing both volatile compounds and water pollutants. They can selectively adsorb molecules that are smaller than their pore sizes, and their large surface areas make them versatile materials for targeting a wide range of pollutants. It has been found that the zeolitized fly ash (ZFA) has promising potential as a molecular sieve in purification treatments of CO_2, SO_2 and NH_3 [2,19,20]. ZFA has been extensively used for reducing the heavy metal content of acidic mine water [21] and for the removal of ammonium, phosphate [22] and arsenate ions [23] from urban and industrial waste water.

Although the adsorption of dyes onto zeolites has been extensively investigated [36–44] only a few studies have been reported about the adsorption of dye onto fly ash-based zeolites [7,12]. It has been shown that the molecular dimensions of thionine (TH) allow it to fit into the main channel of a zeolite L, and it can fill in the cage by ion exchange. However, the related, yet slightly larger methylene blue and ethylene blue molecules cannot be introduced into the channel [43,44]. A comparison of the adsorption capabilities of TH with larger dyes may provide valuable information about adsorption mechanisms and the structure of the zeolites. In this study, the adsorption behavior of TH and the slightly larger safranine T (ST) molecules onto FA were compared, and its three ZAFs products were produced under several hydrothermal conditions.

* Corresponding author. Tel.: +90 212 4737070; fax: +90 212 4737180.
E-mail address: gultena@istanbul.edu.tr (G. Atun).

0304-3894/$ – see front matter © 2011 Elsevier B.V. All rights reserved.
doi:10.1016/j.jhazmat.2011.01.075

2. Materials and methods

2.1. Adsorbate specifications

TH and ST were supplied from Aldrich Chem. Co. (purity, 88%) and Sigma Co. (purity, 90%), and they were used as received. The molecular dimensions of TH and ST were calculated to be 5.00 Å × 11.54 Å and 9.24 Å × 11.29 Å by using the Gaussian 03 software package.

2.2. Adsorbent preparation and specifications

The fly ash sample used to prepare the zeolitic materials was supplied from the Ankara Çayırhan Thermal Power Plant in Turkey, which is fuelled by Beypazarı lignite. The fly ash zeolites were prepared as described previously [19]. Typically, 10 g of FA, 25 g of 3 M NaOH solution, and 2 g of NaCl were mixed and heated to 90 °C and 150 °C in Teflon-lined hydrothermal pressure vessels for varying lengths of time. Three types of zeolitized fly ash (ZFA) were considered, which were maintained at 90 °C for 1 day (ZFA90d1d), 90 °C for 7 days (ZFA90d7d), and 150 °C for 1 day (ZFA150d1d).

X-ray diffraction (XRD) patterns of FA and its zeolitized products are presented in Fig. 1a–d. As shown in Fig. 1a, the FA is mainly composed of a silica-rich glassy phase with minor amounts of mullite ($Al_6Si_2O_{13}$) and quartz (SiO_2) [45]. As can be seen in Fig. 1b–d, the FA was converted into zeolite X (ZX, $Na_2Al_2Si_{2.5}O_{9.6}{\cdot}2H_2O$), zeolite Y (ZY, $Na_2Al_2Si_{4.5}O_{13}{\cdot}9H_2O$), zeolite Na-P1 (Na-P1, $Na_6Al_6Si_{10}O_{32}{\cdot}12H_2O$), analcime (A, $NaAlSi_2O_6{\cdot}H_2O$) and sodalite (S, $Na_8Al_6Si_6O_{24}Cl_2$) type zeolites. These results are consistent with previous investigations, which suggest that the synthesis process is relatively insensitive to the starting material composition, and depend more so on the synthesis temperature and time [19]. The amounts of the zeolites in the samples identified from the XRD patterns was characterized as ZFA90d1d: ZX ≫ S; ZFA90d7d: NaP1 > ZY > ZX > A > S and ZFA150d1d: S > A.

Chemical compositions of FA and ZFA products were determined using a RIGAKU RIX2000 X-ray fluorescence (XRF) spectrometer [16]. The specific surface area and pore properties of the adsorbents were examined by analyzing the data obtained from nitrogen adsorption experiments using a Quantachrome Autosorb Automated Gas Sorption System. The chemical compositions and BET results given in Table 1 suggested that FA partly converted into zeolitic products.

The reported cation exchange capacities (CECs) of the zeolitic materials ZX, ZY, Na-P1, A and S were 4.7, 3.2, 2.7, 0.6 and 0.3 meq/g, respectively [2,20,24]. The pore openings of ZX and ZY were 7.3 Å. The Na-P1 had two openings of 3 and 5 Å. The pore widths of A and S were 2.6 and 2.3 Å, respectively [2]. The particle size distributions of the adsorbents based on mass fraction are presented in Table 2. The mean particle diameters of FA, ZFA90d1d ZFA90d7d and ZFA150d1d adsorbents were estimated as 90, 185, 110 and 75 μm, respectively.

Scanning electron microscopy (SEM) investigations were conducted in a Jeol-JSM 5600 scanning electron microscope to observe the microstructure of the samples before and after hydrothermal treatments. SEM images of FA and ZFA products can be compared in Fig. 2a–d. The FA sample in Fig. 2a was characterized by spherically and irregularly round-shaped. As clearly shown in Fig. 2b–d, an agglomeration is observed in each case and FA undergoes zeolitization after hydrothermal treatments.

2.3. Adsorption experiments

2.3.1. Kinetic studies

Kinetic experiments were conducted in 5×10^{-5} M dye solutions because the calibration plots constructed for concentration

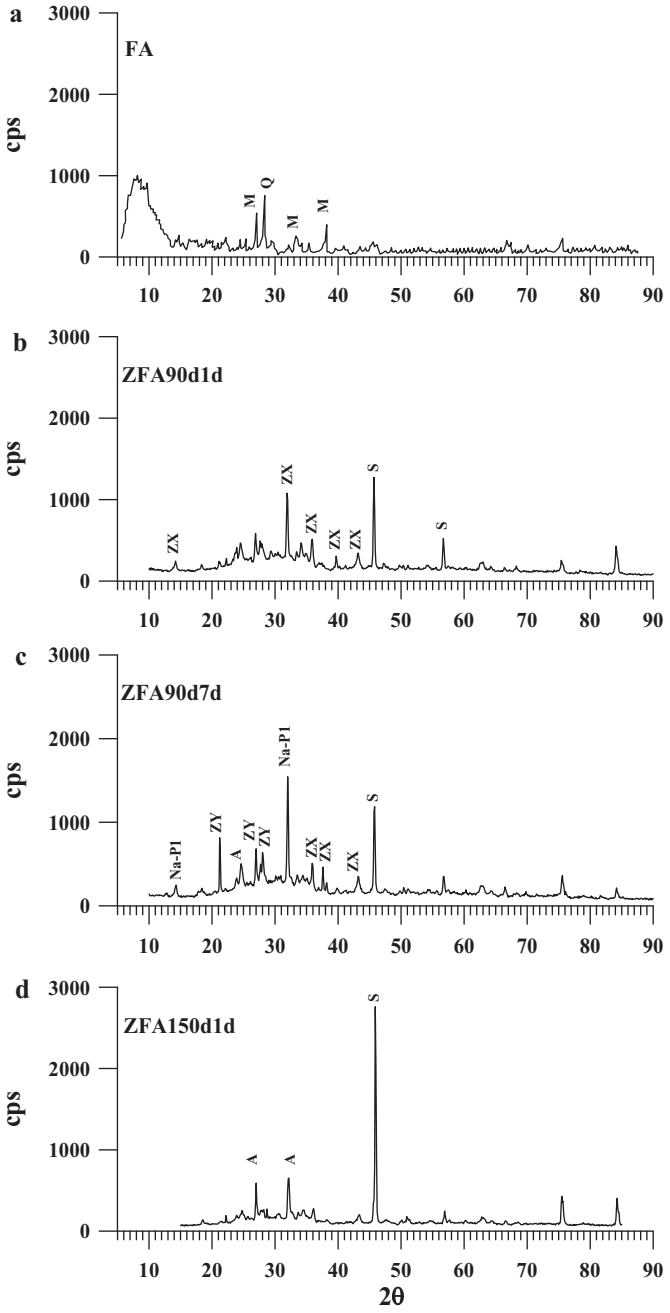

Fig. 1. XRD patterns of the FA and zeolitized FA adsorbents produced at different hydrothermal conditions.

Table 1
Chemical compositions and textural properties of FA and ZFA adsorbents.

	FA	ZFA90d1d	ZFA90d7d	ZFA150d1d
SiO_2	41.30	38.55	36.95	37.55
CaO	16.30	13.86	13.54	13.79
Al_2O_3	12.30	10.95	10.01	10.52
Fe_2O_3	11.30	11.45	11.57	11.96
K_2O	5.62	5.03	4.75	4.83
MgO	4.10	3.67	3.50	3.52
SO_3	5.43	4.62	4.56	4.60
Na_2O	1.43	7.50	6.44	8.25
TiO_2	0.98	0.93	0.88	0.92
S_{BET} (m^2/g)	7.1	28.5	27.4	29.4
V (cm^3)	0.010	0.056	0.065	0.081

Table 2
Particle size distribution based on mass fraction.

Particle size (d, μm)	FA	ZFA90d1d	ZFA90d7d	ZFA150d1d
$d > 350$	0.020	0.219	0.343	0.131
$350 > d > 250$	0.017	0.066	0.063	0.058
$250 > d > 150$	0.114	0.143	0.146	0.220
$150 > d > 70$	0.222	0.381	0.202	0.239
$70 > d > 40$	0.572	0.132	0.171	0.196
$40 > d$	0.055	0.059	0.075	0.156

determination of TH and ST were linear and obeyed Beer's law for both dyes up to this concentration. The concentrations of the dye solutions were determined using the monomer peak absorbances located at 599.0 and at 519.5 nm using a Perkin-Elmer model 554 UV-spectrophotometer. Time dependent experiments were carried out using the batch method at the temperatures of 298, 305, 308 and 318 K. For each individual experiment, 0.1 g of adsorbent was placed into a screw-capped polypropylene vials that was 20 cm^3. Vials containing 10 cm^3 of dye solution were agitated in a thermostatic shaker at 200 rpm for varying time at constant temperature with a precision of ±0.01 °C. The two phases were separated by centrifugation at 4000 rpm and concentration of the solutions was determined.

The time-dependent amount of dye adsorbed (q_t) was calculated from the concentration changes during the adsorption process using the following equation:

$$q_t = (C_0 - C_t)\frac{V}{W} \quad (1)$$

where C_0 and C_t are the molar concentrations of dyes at times zero and t, respectively. V/W is the ratio of the solution to the mass of adsorbent (in L/g).

The pH values of 5×10^{-5} M TH and ST solutions were measured as 6.39 and 6.34, respectively. The effect of solution pH on dye removal at 298 K was investigated by changing the initial pH (2–10) adjusting by HCl or NaOH.

2.3.2. Equilibrium studies

Equilibrium experiments for the construction of adsorption isotherms were carried out at the lowest possible dye concentrations to avoid interactions of dyes in the solutions. Initially, the dye concentration was kept constant at 5×10^{-5} M and solution/adsorbent ratio was changed in the range of 0.0125–2 L/g for ST and 0.0125–6 L/g for TH at 298 K. Then, the dye concentration was increased up to 1.5×10^{-4} M at the highest solution/adsorbent ratio to observe the plateau region on the isotherm curves.

2.3.3. Infrared spectral measurement

The interactions of the dyes with the adsorbents were examined by attenuated total reflectance Fourier-transform infrared (ATR FT-IR) spectroscopy using a Bruker Alpha-P platinum diamond ATR FT-IR spectrometer. The spectra of TH loaded adsorbents at low (I), medium (II) and high (III) loadings were compared with their corresponding bare adsorbents. The loaded samples I and II were prepared using 5×10^{-5} M dye solution at adsorbent dosages of 10 and 2 g/L, respectively. The sample III was loaded with 1.5×10^{-4} M dye solution at a solid/solution ratio of 0.5 g/L. The infrared patterns of ST were recorded at low (I) and high (III) dye loadings. The ATR FT-IR spectra of FA and ZFA samples before and after dye adsorption were presented in Fig. 3a–d and a′–d′ for TH and ST, respectively. As a representative, the spectra of free TH and ST were also compared with ZFA150d1d at low dye loading in Fig. 4a and b, respectively.

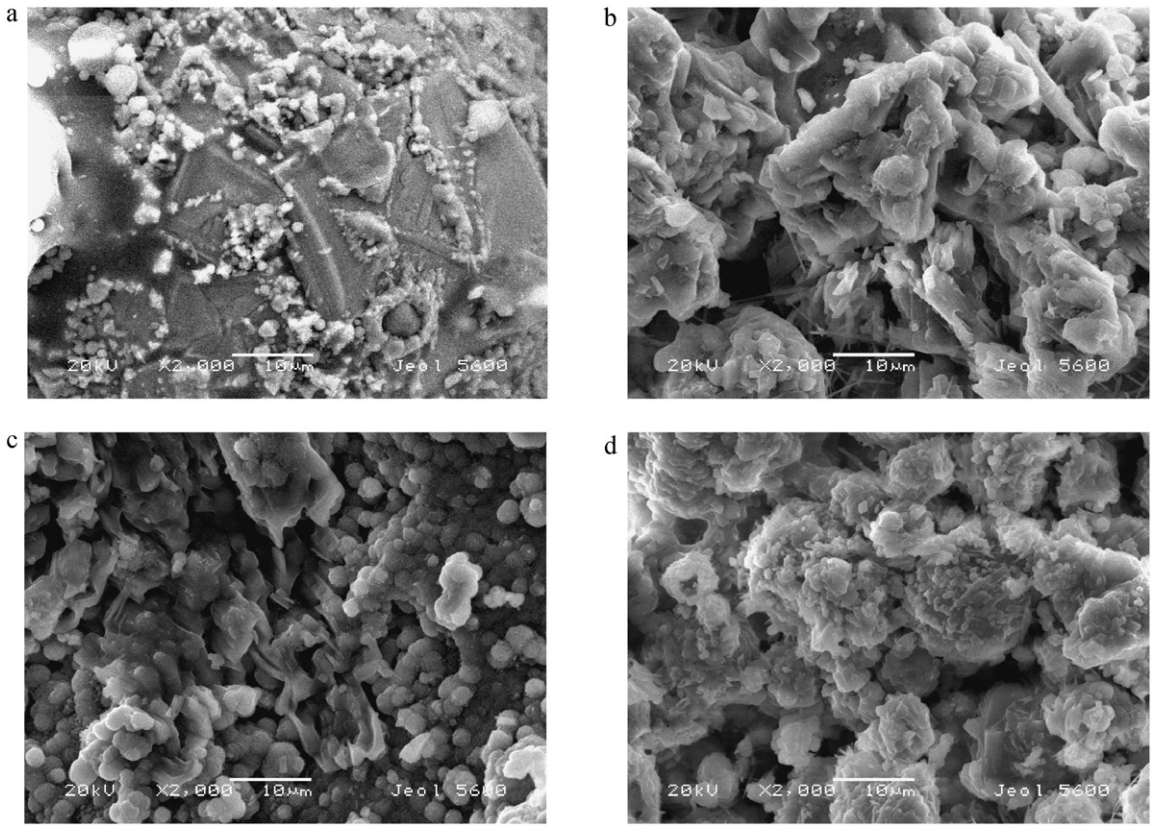

Fig. 2. SEM images of four systems studied: (a) FA, (b) ZFA90d1d, (c) ZFA90d7d and (d) ZFA150d1d.

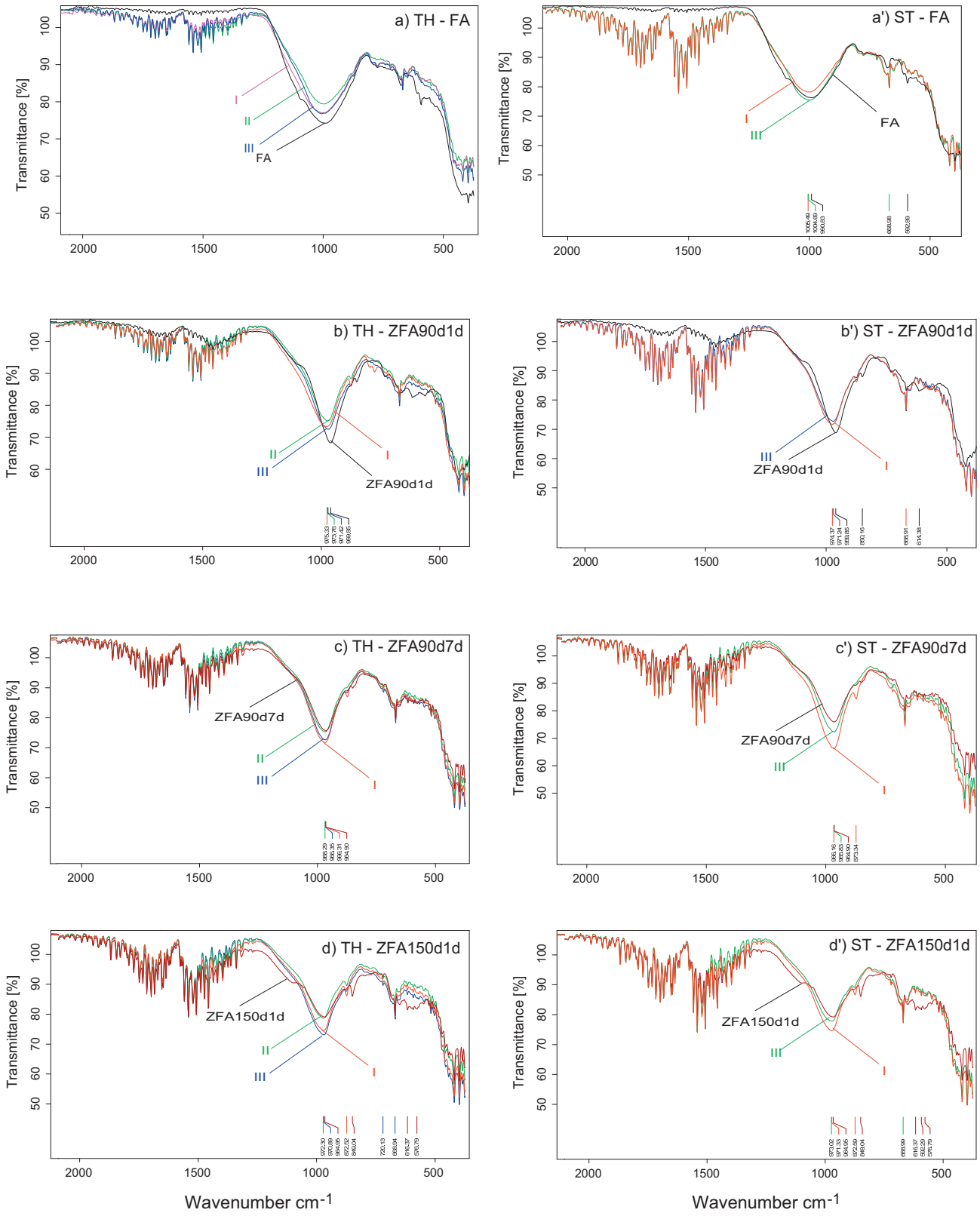

Fig. 3. FT-IR spectra of the adsorbents before and after TH (a–d) and ST (a′–d′) loading.

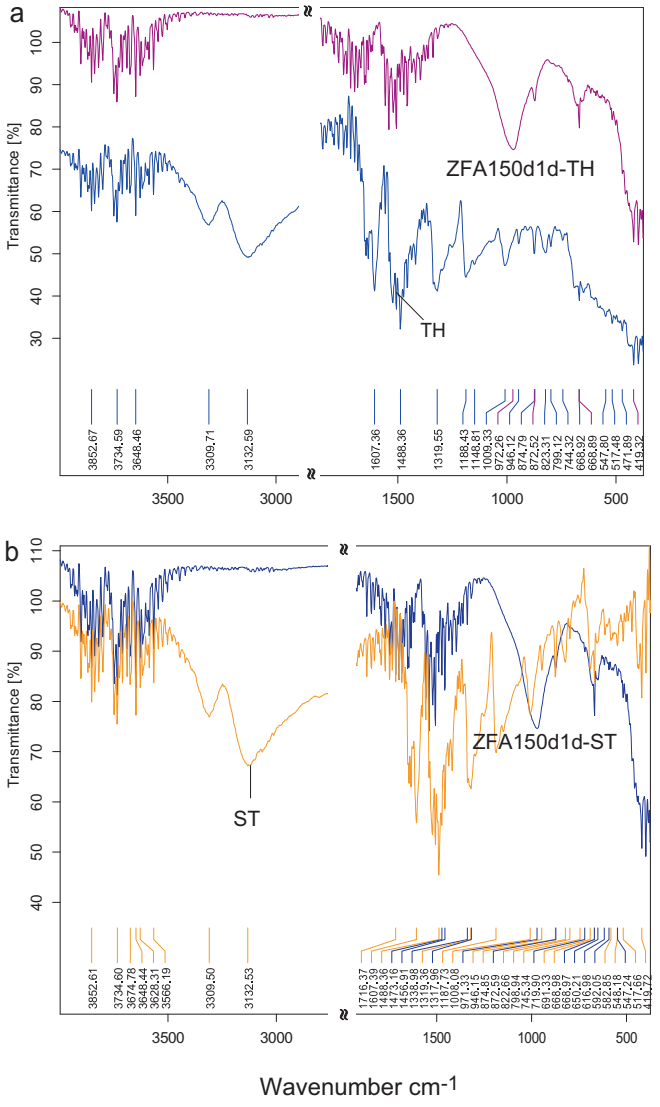

Fig. 4. A comparison of FT-IR spectra of free dyes and dye loaded ZFA150d1d: (a) TH and (b) ST.

3. Results and discussion

3.1. Adsorption kinetics

The data for time dependent TH and ST adsorption onto FA, ZFA90d1d, ZFA90d7d and ZFA150d1d are represented in Figs. 5a–d and 6a–d, respectively.

The data were well approximated by the homogeneous surface diffusion model (HSDM). A single diffusion coefficient was assumed in the model, and the rate-limiting step is surface diffusion. The variation of the solute phase concentration, q, with distance, r, and time, t, for spherical particles, assuming symmetry in two directions, is given by the following equation [46]:

$$\frac{\partial q}{\partial t} = D_s\left(\frac{\partial^2 q}{\partial r^2} + \frac{2}{r}\times\frac{\partial q}{\partial r}\right) \quad (2)$$

Here D_s is the solid phase surface diffusion coefficient.

The initial and boundary conditions for the solution and solid phases are given as:

$$C_t(0) = C_0 \quad (3)$$

$$q_t(r, 0) = 0 \quad (4)$$

$$q(R, t) = q_s(t) \quad (5)$$

$$\frac{\partial q}{\partial t}(0, t) = 0 \quad (6)$$

Here q_s is solid-phase concentration at the particle surface, and R is the radius of adsorbent particles.

Typical adsorption kinetics were described in terms of the fractional approach towards equilibrium, U_t, at time t and were determined experimentally as:

$$U_t = \frac{q_t}{q_e} \quad (7)$$

where q_e is solid phase concentrations of solute at equilibrium.

U_t can be estimated by applying a finite difference technique according to Paterson's and Nernst–Plank's (N–P) approximations.

3.1.1. Paterson's approximation

The exact solution of Eq. (4) for a limited bath technique (finite solution volume) is:

$$U_t = 1 - \frac{2}{3w}\sum_{n=1}^{\infty}\frac{\exp(-S_n^2 P)}{1 + S_n^2/9w(w+1)} \quad (8)$$

where S_n is the root of the equation.

$$S_n \cot S_n = 1 + \frac{S_n^2}{3w} \quad (9)$$

The following approximation was proposed by Paterson for the solution of Eq. (4) [47]:

$$U_t = \frac{w+1}{w}(1 - f_1[f_2(1+f_3) - f_4(1+f_5)]) \quad (10)$$

where $f_1 = 1/(a-b)$, $f_2 = a\exp(a^2P)$, $f_3 = \mathrm{erf}(aP^{1/2})$, $f_4 = b\exp(b^2P)$, $f_5 = \mathrm{erf}(bP^{1/2})$; a and b roots of equation: $x^2 + 3wx - 3w = 0$ $(a > b)$, $w = \overline{C_e}\overline{V}/C_eV$, $\overline{C_e}$ and C_e are equilibrium concentrations in solid and solution phases and $\overline{V}$ is the volume of the solid phase, and $P = D_s t/R^2$.

The values of U_t have been computed from Paterson's approximation by minimizing the standard deviations between the experimental and calculated q_t values according to:

$$\sigma = \left[\frac{1}{n_e}\sum_{i=1}^{n}(q_{t,\exp} - q_{t,cal})^2\right]^{0.5} \quad (11)$$

where n_e is the number of experimental observations; the subscripts "exp" and "mod" are the experimental and modeled values of q_t, respectively.

The values of D_s and q_e were calculated using Paterson's approximation and the standard deviations are presented in Table 3 for TH and ST adsorption systems. The modeled curves (dashed lines) were compared with the experimental points in Figs. 5a and 6a–d, respectively. As can be seen from the figures, Paterson's approximation could be applied to ST adsorption for all adsorbents, whereas only the FA–TH adsorption system can be described by the approximation. The magnitude of D_s values for ST adsorption onto all adsorbents is $\sim 10^{-13}$ m^2/s where they fall into 10^{-12} to 10^{-11} m^2/s for TH onto zeolitized products of fly ash. This suggests that this approximation is applicable to model the relatively slower adsorption process.

Higher values of the diffusion coefficient for TH indicate that the smaller TH molecules can more easily access the pores. As it is seen in Fig. 5a, the amount of TH adsorbed onto FA increases rapidly until 30 min and then gradually decreases. Similar behavior has been reported for some dye–adsorbent systems [48]. The functional form of the kinetic curve can be predicted using only the Paterson's approximation.

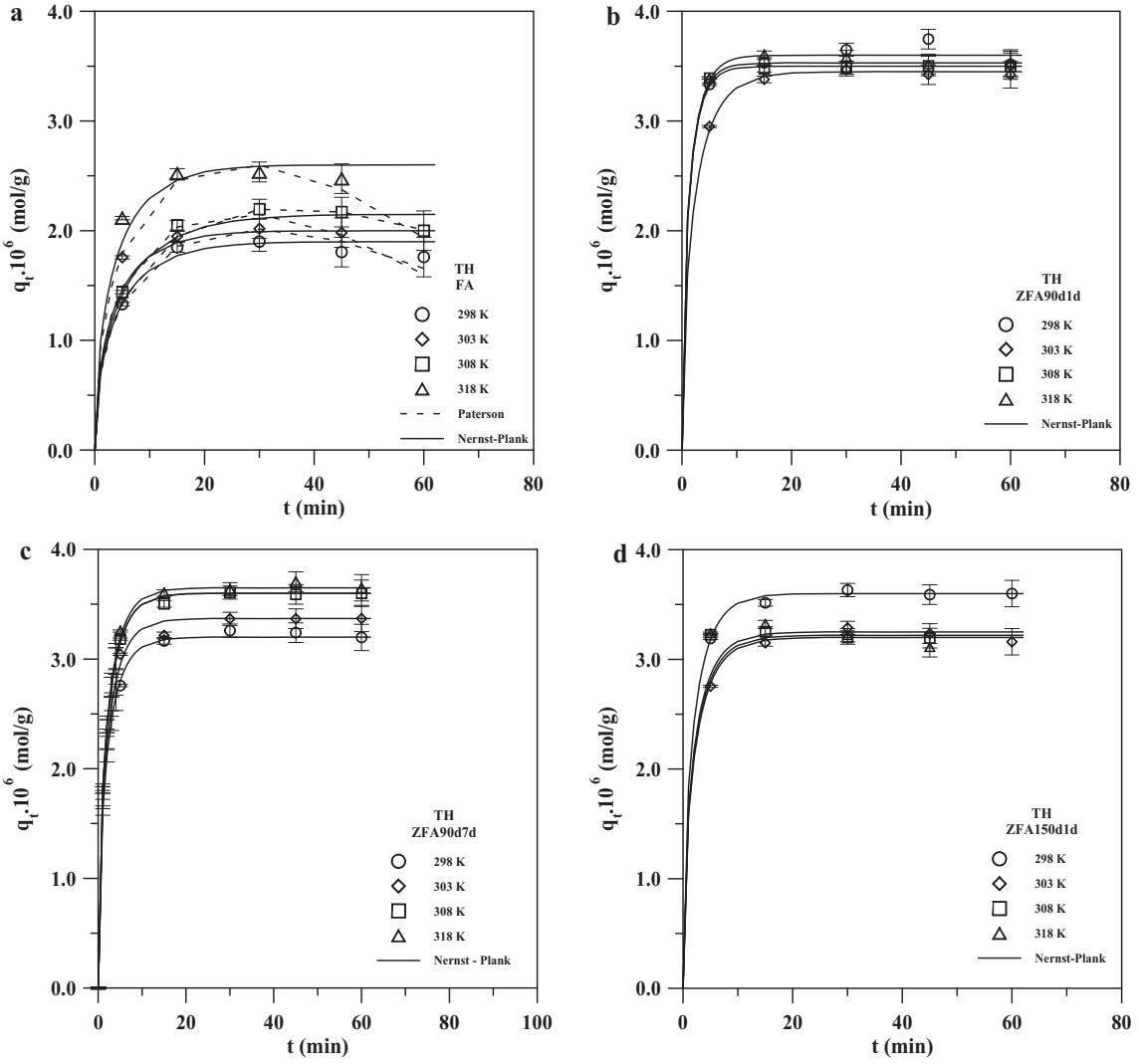

Fig. 5. Time-dependence of the TH adsorption onto FA and its zeolitized adsorbents prepared under different hydrothermal conditions (solid and dashed lines have been modeled according to Nernst–Plank's and Paterson's approximations, respectively).

The diffusion coefficients of both dyes increase with temperature for FA, ZFA90d1d and ZFA90d7d whereas an opposite behavior is observed for ZFA150d1d.

The removal mechanism of dyes may be elucidated by considering the FT-IR spectra of the adsorbent before and after dyes adsorption in Figs. 3a–d and 4a for TH as well as in Figs. 3a′–d′ and 4b for ST. The curves (*I*) for low loadings correspond to equilibrium adsorption of time dependent experiments at 298 K.

As shown from the figures, the two most intense bands for fly ash zeolites usually occur at 1300–800 cm^{-1} and 500–400 cm^{-1} of the IR patterns. The first can be assigned to an asymmetric stretching and the second one to a bending mode of the T–O bond. The peaks are located at approximately 1700–1450 cm^{-1} for O–H bending. The band at 420–400 cm^{-1} is assigned to pore opening on external linkage. The pseudo-lattice bands between 800 and 500 cm^{-1} are associated with the presence of rings containing different numbers of units [25,49].

The band at 990 cm^{-1} in Fig. 3a and a′ is associated with the vitreous component of the FA. The bands at 965 and 849 cm^{-1} in Fig. 3b–d and b′–d′ can be assigned to Si–O-terminal vibrations and shoulder at 1140–1010 cm^{-1} to Si–O–Si bridge vibrations. As the curing temperature increases the intensity of the bands in the Si–O–Si bridge bonds grows with respect to the intensity of bands attributed to the Si–O-terminal bonds.

The absorption bands at 1607 and 1488 cm^{-1}, as shown by the curve of free TH in Fig. 4a, are assigned to the skeletal vibration of the phenyl ring of TH, which are also shown by the adsorbed TH curve, confirming the presence of TH on the ZFA150d1d surfaces [49]. The absorption bands at 3309 and 3132 cm^{-1} are ascribed to the N–H stretching vibration of the amino moieties, which are not observed in the IR spectrum of the adsorbed TH curve, indicating that the nitrogen atoms of the NH_2 moieties of TH bind strongly to adsorbent surfaces [50]. Similar behavior is also observed for ST as shown in Fig. 4b.

As can be seen in Fig. 3d and d′, shoulder at 1140–1010 cm^{-1} belonging to Si–O–Si bridge vibrations disappears after dye loading indicating dye adsorption in internal tetrahedral of ZFA150d1d. On the other hand, the bands at 965 and 849 cm^{-1} shift towards higher frequencies. This behavior is an indication of interactions between dye and Si–O-terminal bonds. Intensities of the shoulders for ZFA90d1d and ZFA90d7d in Fig. 3b–c and b′–c′ are lower than those of ZFA150d1d in Fig. 3d and d′ and the bands moved to higher frequencies after dye loading exhibit more effective dye – Si–O-interactions. It can be concluded that the rate of adsorption processes onto ZFA adsorbents may be controlled by both Si–O–Si and Si–O-interactions with dyes. The inverse temperature dependence suggests that rate limiting step is dye – Si–O–Si interactions onto ZFA150d1d whereas the rate of

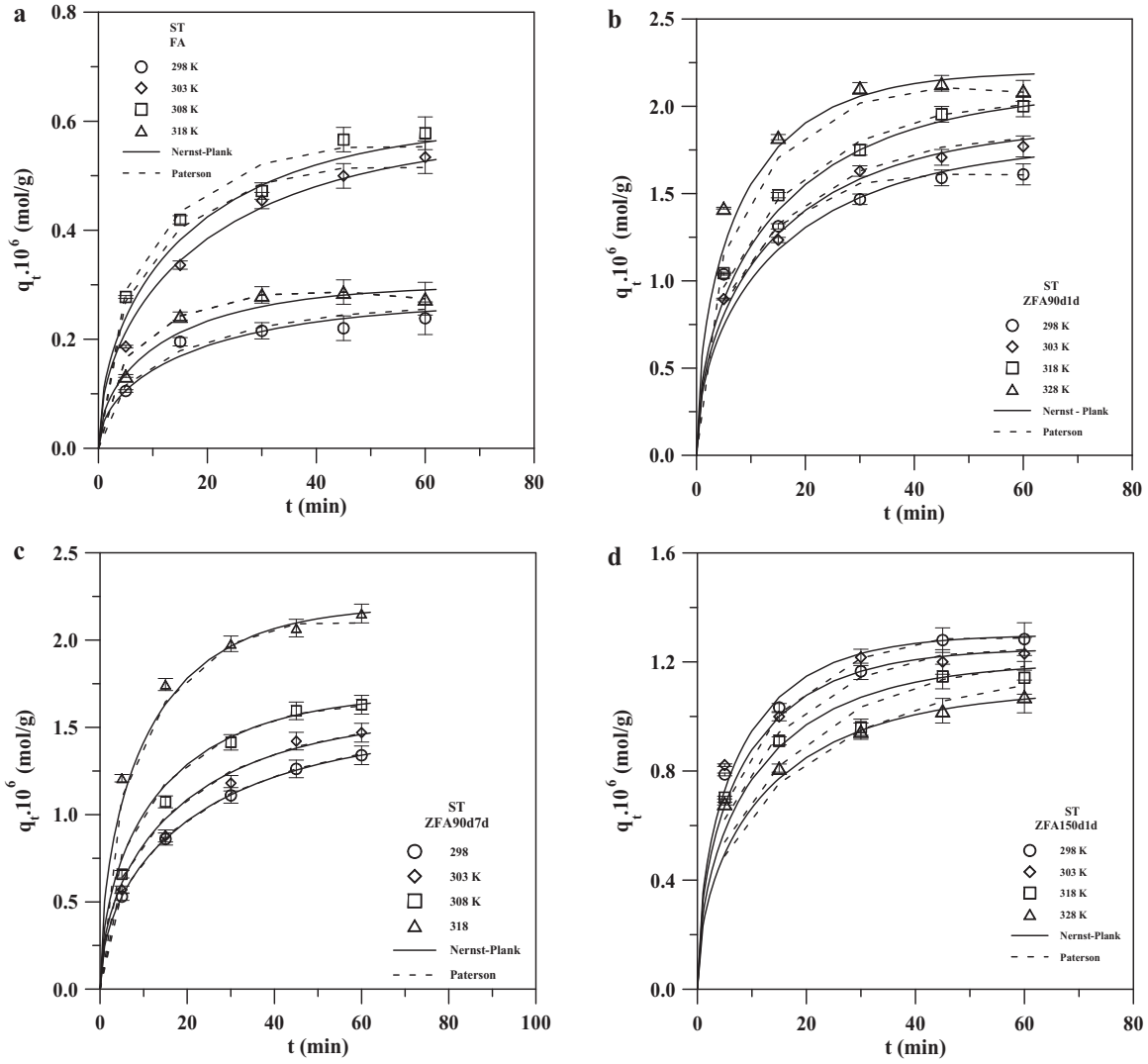

Fig. 6. Time-dependence of ST adsorption onto FA and its zeolitized adsorbents produced under different hydrothermal conditions (solid and dashed lines have been modeled according to Nernst–Plank's and Paterson's approximations, respectively).

Table 3
Kinetic parameters for TH and ST adsorption onto FA and ZFA adsorbents.

Sample	T (K)	TH				ST			
		D_s (m^2/s)	$q_e \times 10^6$ (mol/g)	$\sigma_{Paterson}$	σ_{N-P}	$D_s \times 10^{13}$ (m^2/s)	$q_e \times 10^6$ (mol/g)	$\sigma_{Paterson}$	σ_{N-P}
FA	298	3.04×10^{-13}	2.03	0.056	0.091	1.62	0.29	0.248	0.221
	303	3.65×10^{-13}	2.13	0.249	0.220	2.03	0.58	0.213	0.219
	308	4.05×10^{-13}	2.23	0.185	0.156	2.43	0.60	0.027	0.029
	318	4.46×10^{-13}	2.66	0.637	0.813	3.24	0.30	0.015	0.018
ZFA90d1d	298	5.08×10^{-12}	3.60	–	0.085	5.92	1.70	0.079	0.151
	303	8.46×10^{-12}	3.45	–	0.029	6.77	1.90	0.055	0.052
	308	9.31×10^{-12}	3.50	–	0.035	7.11	2.10	0.044	0.081
	318	1.02×10^{-11}	3.53	–	0.080	8.46	2.20	0.136	0.115
ZFA90d7d	298	1.20×10^{-11}	3.20	–	0.036	6.05	1.50	0.017	0.004
	303	1.23×10^{-11}	3.37	–	0.038	7.26	1.58	0.069	0.058
	308	1.28×10^{-11}	3.60	–	0.073	9.68	1.70	0.074	0.061
	318	1.35×10^{-11}	3.65	–	0.040	12.10	2.20	0.071	0.083
ZFA150d1d	298	2.25×10^{-12}	3.60	–	0.033	5.63	1.32	0.056	0.043
	303	2.19×10^{-12}	3.25	–	0.073	5.06	1.27	0.099	0.071
	308	2.14×10^{-12}	3.22	–	0.187	3.94	1.22	0.092	0.076
	318	2.08×10^{-12}	3.20	–	0.221	3.38	1.15	0.093	0.085

adsorption is dominated by dye – Si–O-interactions on the other adsorbents.

3.1.2. Nernst–Plank's approximation

In order to determine U_t according to the Nernst–Plank's approximation based on ion exchange, the following equation is employed [51]:

$$U_t = [1 - \exp(m)]^{1/2} \tag{12}$$

with

$$m = \pi^2(c_1 P + c_2 P^2 + c_3 P^3) \tag{13}$$

where the constants c_1, c_2 and c_3 are functions of β. The constants were calculated as follows by minimizing standard deviation between experimental and modeled q_t values:

$$c_1 = -\frac{10}{0.01 + 0.2\beta^{0.92}} \tag{14}$$

$$c_2 = -\frac{1}{0.94 - 2\beta^{0.4635}} \tag{15}$$

$$c_3 = -\frac{1}{0.27 + 0.09\beta^{1.14}} \tag{16}$$

Here β is the ratio of diffusion coefficients of the exchanging species.

The values of β used to obtain the D_s and q_e values predicted by Paterson's approximation for TH adsorption systems were 1, 2, 2 and 1 for FA, ZFA90d1d, ZFA90d7d and ZFA150d1d, respectively. They decrease in the order of 3, 2, 1.5 and 1 for ST adsorption on the same adsorbents. The modeled curves in Figs. 5a–d and 6a–d and standard deviations presented in Table 3 show that all adsorption systems adequately well predicted by Nernst–Plank approximation.

The equilibrium values of TH adsorbed were $(2.03–2.66) \times 10^{-6}$, $(3.45–3.60) \times 10^{-6}$, $(3.20–3.65) \times 10^{-6}$ and $(3.60–3.20) \times 10^{-6}$ mol/g for FA, ZFA90d1d, ZFA90d7d and ZFA150d1d in temperature range of 298–318 K.

The values of q_e for ST onto FA regularly increased from 0.29×10^{-6} to 0.60×10^{-6} mol/g in 298–308 K range, and a decrease was observed at the highest temperature of 318 K. A similar temperature dependence was reported for TB adsorption onto FA [13]. The equilibrium values of ST onto ZFA90d1d, ZFA90d7d and ZFA150d1d are $(1.70–2.20) \times 10^{-6}$, $(1.50–2.20) \times 10^{-6}$ and $(1.32–1.15) \times 10^{-6}$ mol/g, respectively. The lower q_e values for ST can be correlated to its larger molecular size than that of ST.

3.2. Thermodynamic parameters

Thermodynamic parameters for dye–adsorbent systems at the transition state were evaluated from the temperature dependencies of the surface diffusion coefficients using the linearized Eyring equation [52]:

$$\ln \frac{D_s}{T} = Ln2.72d^2 \frac{k}{h} + \frac{\Delta S^*}{R} - \frac{\Delta H^*}{T} \tag{17}$$

where k and h are Boltzmann and Planck constants, T is the absolute temperature, R is the gas constant (kJ/mol K), d is the average distance between the successive adsorption sites ($\sim 10^{-10}$ m), and ΔS^* and ΔH^* the entropy and the enthalpy of activation, respectively.

The values of ΔH^* and ΔS^* for TH and ST systems have been calculated from the slope and the intercept of the Eyring plots in Fig. 7a and b, respectively. The Gibbs free energies of activation ΔG^* have been computed using the following equation:

$$\Delta G^* = \Delta H^* - T\Delta S^* \tag{18}$$

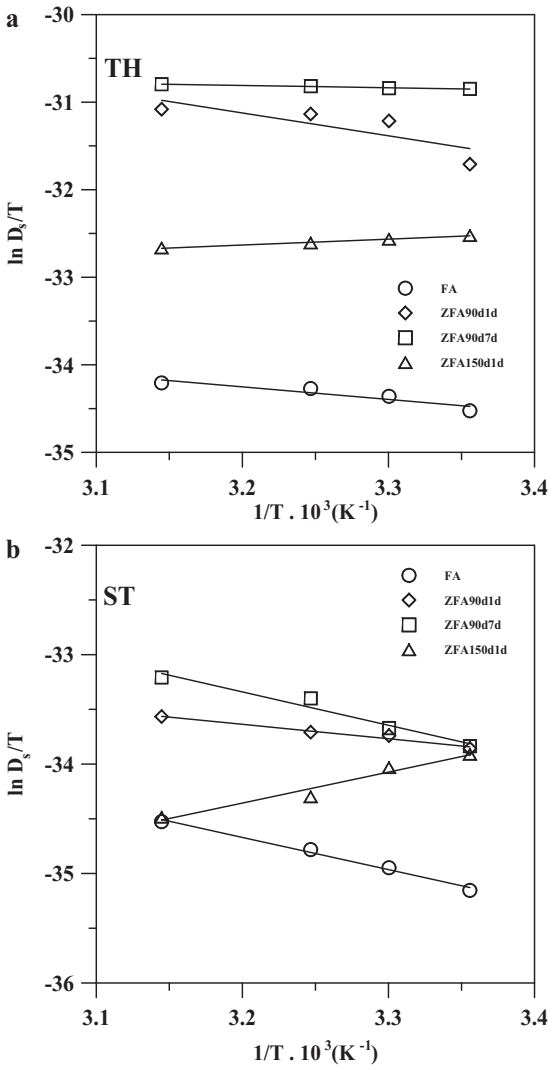

Fig. 7. Eyring plots for calculation of the thermodynamic parameters at transition states of the dyes: (a) TH and (b) ST.

Values of thermodynamic parameters for transition states of TH and ST are also presented in Table 4. As can be inferred from Table 4, the adsorption processes are endothermic for FA, ZFA90d1d and ZFA90d7d, but not for ZFA150d1d.

The endothermic nature of the systems may be arising from strong dye – Si–O-interactions whereas the exothermic nature may be attributed to dye – Si–O–Si interactions in the activated state.

The negative values of ΔS^* imply that the transition state is more ordered than the initial state and no significant change occurs in the internal structure of the adsorbents. The positive free energy changes indicate the presence of an energy barrier in all systems which may partially arise from hydration of the dyes in solution [53]. When the dyes adsorb to the particle surface from solution, at least some of the water molecules forming a hydration shell of dye cations are shed.

3.3. Effects of pH on dye adsorption

Fig. 8 displays the influence of pH on dye adsorption at various initial solution pH under the same conditions with kinetic experiments. Adsorption of two dyes on the FA slightly increases at lower pH and a sharp increment is observed above pH 9. On the other hand, dye adsorption onto ZFA products slightly depends on pH and nearly constant in the pH range of 5–10. Similar findings reported

Table 4
Thermodynamic parameters for activated states of the dyes.

	ΔH^* (kJ/mol)	ΔS^* (kJ/mol K)	ΔG^* (kJ/mol)				r
			298 K	303 K	308 K	318 K	
TH							
FA	11.91	−0.070	32.64	32.99	33.34	34.03	0.933
ZFA90d1d	21.69	−0.123	25.35	25.41	25.47	25.59	0.815
ZFA90d7d	2.18	−0.072	23.67	24.04	24.44	25.12	1.000
ZFA150d1d	−5.63	−0.112	27.81	28.37	28.93	30.05	0.997
ST							
FA	24.44	−0.033	34.27	34.43	34.60	34.93	0.995
ZFA90d1d	10.95	−0.068	31.08	31.42	31.76	32.43	0.987
ZFA90d7d	25.32	−0.019	31.01	31.11	31.20	31.40	0.980
ZFA150d1d	−23.53	−0.184	31.29	32.21	33.13	34.97	0.980

for MB adsorption have been attributed to adsorption of dyes on ionizable surface of the FA with different origin [5,8–10] while dye is adsorbed on pH independent ion exchange sites of zeolite [54].

3.4. Adsorption equilibria

3.4.1. Adsorption isotherms of TH

The adsorption isotherms of TH in Fig. 9a typically display two plateau regions. A two-step adsorption isotherm can be better analyzed on a log–log scale corresponding to the Freundlich isotherm [55]:

$$\log q_e = \log k_F + n \log C_e \quad (19)$$

where k_F and n are Freundlich constants, which describe the adsorption capacity and surface heterogeneity, respectively.

A linearized plot of the two-step adsorption isotherm yields four straight lines whose slopes obey $n_1 > n_2 < n_3 > n_4$ [56]. The values of n obtained from the Freundlich isotherms in Fig. 9b for TH–FA and ZFA systems are shown in Table 5. The order of the n values presented in Table 5 is consistent with previous investigations [13,56].

The values of $n_1 > 1$ correspond to the initial portion of an S shaped adsorption isotherm. The low surface excess in this region can be attributed to a competition between dye and water molecules for adsorption sites. Strong medium bands at about 1700–1450 cm^{-1} attributed to the presence of the H_2O mode and incomplete dehydration of the zeolite samples. However, it cannot be clearly shown dye–water competition because these bands overlap with aromatic skeletal vibration bands of dyes at 1607 and 1488 cm^{-1}.

The second region in Fig. 9b corresponds to the first plateau in Fig. 9a. The adsorption capacities of TH estimated from the plateau region are 0.45×10^{-5}, 0.90×10^{-5}, 0.75×10^{-5} and 0.85×10^{-5} mol/g for FA, ZFA90d1d, ZFA90d7d and ZFA150d1d, respectively. Even though different types of the zeolitized prod-

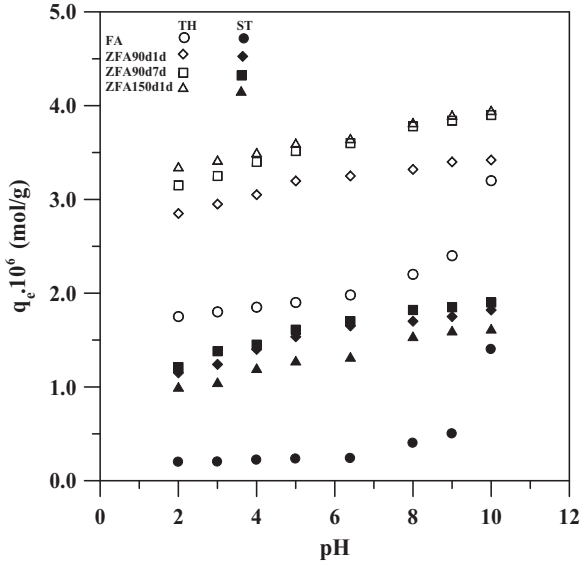

Fig. 8. Effect of pH on dye adsorption in 5×10^{-5} M dye solution at 10 g/L adsorbent dosage.

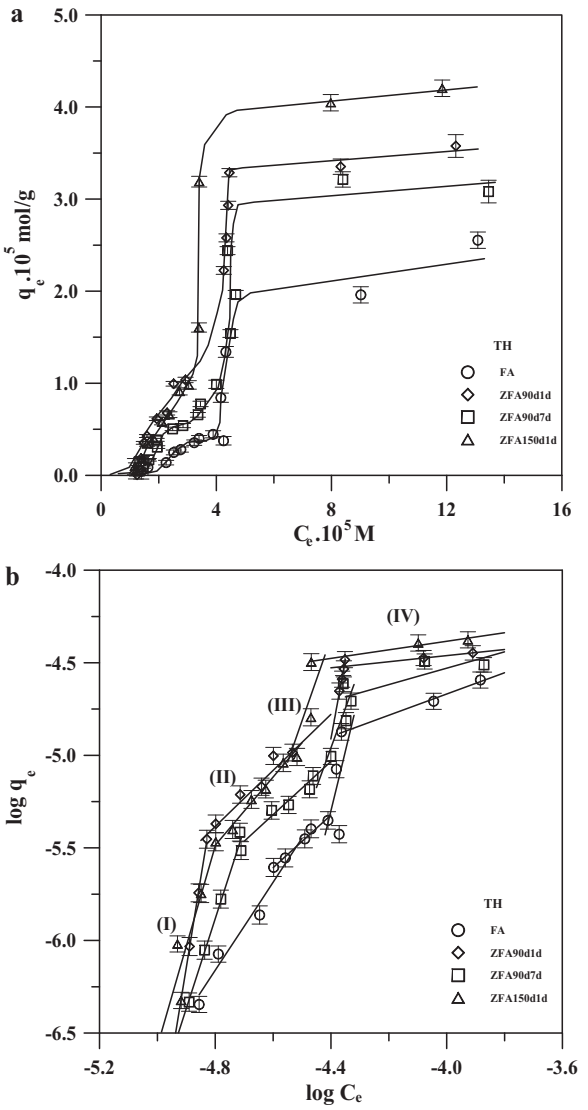

Fig. 9. Adsorption isotherms of TH onto FA and zeolitized FA adsorbents (a) on a linear scale and (b) on a log–log scale.

Table 5
The values of the *n* parameter evaluated from the Freundlich isotherms for TH and ST interacting with FA and its zeolitized adsorbents.

Dye	Sample	Regions	Experimental points	*n*	*r*
TH	FA	1	7	2.38	0.99
		2	5	1.42	0.99
		3	4	6.45	0.52
		4	3	0.57	1.00
	ZFA90d1d	1	4	9.65	1.00
		2	4	1.51	0.97
		3	4	8.59	0.99
		4	3	0.16	1.00
	ZFA90d7d	1	5	4.84	0.99
		2	5	1.48	0.96
		3	4	4.28	0.75
		4	3	0.44	0.86
	ZFA150d1d	1	4	5.41	0.91
		2	5	1.84	0.99
		3	4	4.45	0.82
		4	3	0.23	0.98
ST	FA	1	11	23.75	0.92
		2	3	0.22	0.98
	ZFA90d1d	1	10	20.00	0.93
		2	3	0.16	0.97
	ZFA90d7d	1	11	7.79	0.95
		2	3	0.12	0.95
	ZFA150d1d	1	9	20.31	0.93
		2	3	0.09	0.98

ucts are formed the capacities of ZFA adsorbents are around two times that of the raw fly ash. The order of adsorbent capacities is in agreement with the BET results in Table 1. These results suggest that raw fly ash is partly converted into the zeolitic products during an alkaline hydrothermal process.

The second plateau regions of the isotherm curves occur around 2.25×10^{-5}, 3.60×10^{-5}, 3.00×10^{-5} and 4.25×10^{-5} mol/g for FA, ZFA90d1d, ZFA90d7d and ZFA150d1d, respectively.

The curves II and III in FT-IR spectra in Fig. 3b–d correspond to the first plateau and the second plateau regions, respectively. The intensity of the bands of curves (II) was suppressed with respect to corresponding bands of curves (I) whereas increasing intensity was observed for curves (III). The lower intensity of the curves may be attributed to a stronger interaction of Si–O-terminal bonds and Si–O–Si bonds with dyes or vice versa. Thus, it can be concluded that TH molecules are loosely bound to the surface in the second plateau region.

3.4.2. Adsorption isotherms of ST

As it is seen in Fig. 10a, S shaped isotherms are observed for ST adsorption onto FA and ZFA adsorbents. The Freundlich isotherms in Fig. 10b, yield two straight lines with decreasing slopes. The *n* values, which correspond to the slopes of the first, and the second straight lines are also presented in Table 5. The adsorption capacities of the adsorbents can be identified from the plateau in Fig. 10a.

The ST capacity of FA (0.45×10^{-5} mol/g) was equal to its TH capacity at the first plateau. This indicates that both dyes are adsorbed onto the same adsorption site on the surface in the low concentration region. The adsorption capacity of ST of 1.80×10^{-5} mol/g for ZFA90d1d is two-fold higher than that of TH of 0.90×10^{-5} mol/g at the first plateau. The adsorption capacities of ZFA90d7d and ZFA150d1d for ST are 2.00×10^{-5} and 1.50×10^{-5} mol/g, respectively.

As shown in Fig. 3b′–d′, the intensity of the bands of ST curves (III) corresponding to the plateau region was also decreased with respect to curves (I), just like in the first plateau of TH (i.e., curves (II)).

Adsorption capacities for TH and ST of the zeolitized adsorbents are compared with some cationic dyes onto other zeolitic materials

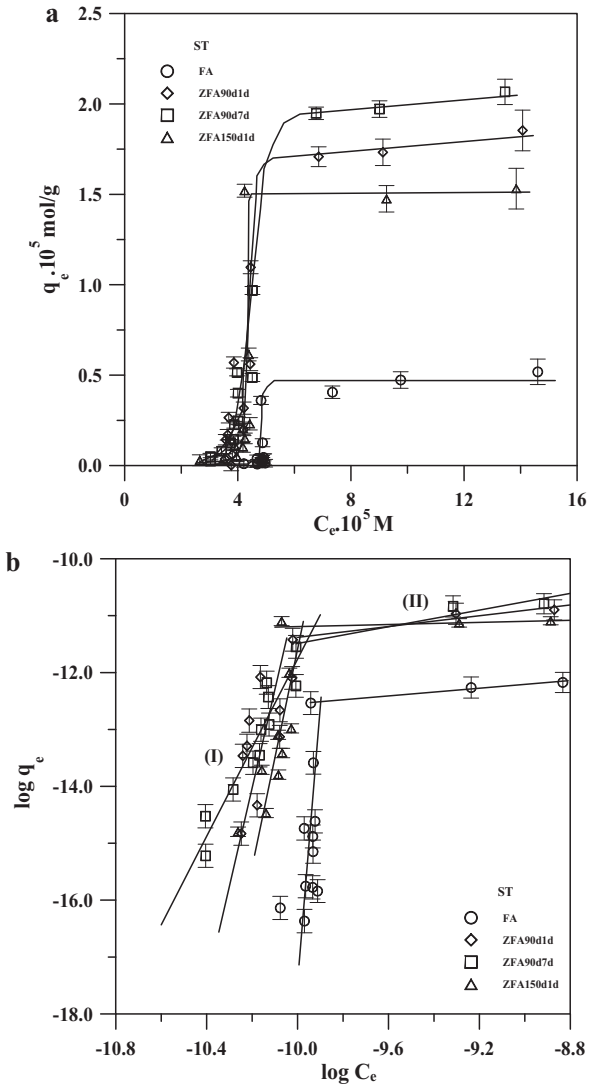

Fig. 10. Adsorption isotherms of ST onto FA and zeolitized FA adsorbents (a) on a linear scale and (b) on a log–log scale.

Table 6
A comparison of adsorption capacities of zeolitized fly ash products for cationic dyes.

	Dye	NaOH	Curing temperature, *t* (°C)	Time	*q* (mol/g)	
ZFA90d1d	TH	3 M	90	1 d	3.60×10^{-5}	This study
ZFA90d7d	TH	3 M	90	7 d	3.00×10^{-5}	This study
ZFA150d1d	TH	3 M	150	1 d	4.25×10^{-5}	This study
ZFA90d1d	ST	3 M	90	1 d	1.80×10^{-5}	This study
ZFA90d7d	ST	3 M	90	7 d	2.00×10^{-5}	This study
ZFA150d1d	ST	3 M	150	1 d	1.50×10^{-5}	This study
FA-100	MB	5 M	100	1 d	4.46×10^{-5}	[10]
FA-140	MB	5 M	140	1 d	5.32×10^{-5}	[10]
FA-140	RB	5 M	140	1 d	3.98×10^{-6}	[10]
FA zeolite	MB	7 M	–	21 h	3.38×10^{-5}	[7]
FA-550	MB	Solid	550	1 h	1.00×10^{-4}	[12]
FA	CV	Solid	550	1 h	1.00×10^{-4}	[12]

derived from fly ash in Table 6. Our results are comparable with the MB capacities of the zeolitic products in Refs. [7,10].

4. Conclusions

The adsorption kinetics and equilibria of two basic dyes TH and ST were studied onto FA and its three zeolitic products obtained

under alkaline hydrothermal conditions. The amounts of zeolite X, zeolite Y, Na-P1, analcime and sodalite formed in the products decrease in the order ZFA90d1d, ZFA90d7d and ZFA150d1d, which were prepared by increasing the curing time and temperature.

The magnitudes of the surface diffusion coefficients of ST were calculated using Paterson's and Nernst Plank's approximations as $\sim 10^{-13}$ m^2/s for all adsorbents. Although the values of D_s for TH onto FA are the same order as those obtained for ST, they increase up to 100 times for the zeolitic adsorbents. The higher diffusion coefficients of TH relative to ST can be rationalized by its smaller size, which can more readily fit into the pores of the zeolitic products involved.

Positive values of ΔH^* for all of the dyes except for the ZFA150d1d adsorbent indicate that the primary mode of the adsorption process is dye – Si–O-interactions. The energy barrier present in the activated state may arise from the negative entropy changes of the activated state because of a regular distribution of the dyes on the adsorbent.

One and two-step isotherm curves were observed for ST and TH, respectively. The S shaped isotherm profile of an initial part of both curves can be attributed to a competition between dyes and water molecules for the same adsorption sites on the adsorbents at low dye concentrations. Freundlich isotherm plots of ST and TH yield two and four straight lines, respectively.

Zeolitized fly ash products can be successfully used as low cost adsorbents for cationic dyes. The highest dye removal was observed at 318 K on FA, ZFA90d1d and ZFA90d7d except for ST–FA system whereas dye adsorption onto ZFA150d1d was more efficient at 298 K. Equilibrium and kinetic results obtained in this study may be useful for designing a treatment plant for dye removal from industrial colored effluents.

References

[1] Z. Jing, N. Matsuoka, F. Jin, N. Yamasaki, K. Suzuki, T. Hashida, Solidification of coal fly ash using hydrothermal processing method. A novel method of advanced materials processing, J. Mater. Sci. 41 (2006) 1579–1584.

[2] X. Querol, N. Moreno, J.C. Umana, A. Alastuey, E. Hernandez, A. Lopez–Soler, F. Plana, Synthesis of zeolites from coal fly ash: an overview, Int. J. Coal Geol. 50 (2002) 413–423.

[3] H. Mimura, K. Yokota, K. Akiba, Y. Onodera, Alkali hydrothermal synthesis of zeolites from coal fly ash and their uptake properties of cesium ion, J. Nucl. Sci. Technol. 38 (2001) 872–878.

[4] R. Apak, G. Atun, K. Güçlü, E. Tütem, Sorptive removal of cesium-137 and strontium-90 from water by unconventional sorbents. II. Usage of coal fly ash, J. Nucl. Sci. Technol. 33 (1996) 365–450.

[5] P. Janos, H. Buchtova, M. Ryznarov, Sorption of dyes from aqueous solutions onto fly ash, Water Res. 37 (2003) 4938–4944.

[6] V.V.B. Rao, S. Rao, S.R.M. Rao, Adsorption studies on treatment of textile dyeing industrial effluent by flyash, Chem. Eng. J. 116 (2006) 77–84.

[7] C.D. Woolard, J. Strong, C.R. Erasmus, Evaluation of the use of modified coal ash as a potential sorbent for organic waste streams, Appl. Geochem. 17 (2002) 1159–1164.

[8] S. Wang, Y. Boyjoo, A. Choueib, A comparative study of dye removal using fly ash treated by different methods, Chemosphere 60 (2005) 1401–1407.

[9] S. Wang, Y. Boyjoo, A. Choueib, Z.H. Zhu, Removal of dyes from aqueous solution using fly ash and red mud, Water Res. 39 (2005) 129–138.

[10] S. Wang, M. Soudi, L. Li, Z.H. Zhub, Coal ash conversion into effective adsorbents for removal of heavy metals and dyes from wastewater, J. Hazard. Mater. B 133 (2006) 243–251.

[11] K.V. Kumar, V. Ramamurthi, S. Sivanesan, Modeling the mechanism involved during the sorption of methylene blue onto fly ash, J. Colloid Interface Sci. 284 (2005) 14–21.

[12] L. Li, S. Wang, Z. Zhu, Geopolymeric adsorbents from fly ash for dye removal from aqueous solution, J. Colloid Interface Sci. 300 (2006) 52–59.

[13] R.Y. Talman, G. Atun, Effects of cationic and anionic surfactants on the adsorption of toluidine blue onto fly ash, Colloid Surf. A 281 (2006) 15–22.

[14] M. Matheswaran, T. Karunanithi, Adsorption of chrysoidine R by using fly ash in batch process, J. Hazard. Mater. 145 (25) (2007) 154–161.

[15] S. Wang, H. Li, Dye adsorption on unburned carbon: kinetics and equilibrium, J. Hazard. Mater. 126 (2005) 71–77.

[16] S. Pura, G. Atun, Adsorptive removal of acid blue 113 and tartrazine by fly ash from single and binary dye solutions, Sep. Sci. Technol. 44 (2009) 75–101.

[17] K. Ravikumar, S. Krishnan, S. Ramalingam, K. Balu, Optimization of process variables by the application of response surface methodology for dye removal using a novel adsorbent, Dyes Pigments 72 (2007) 66–75.

[18] Z. Eren, F.N. Acar, Adsorption of reactive black 5 from aqueous solution: equilibrium and kinetic studies, Desalination 194 (2006) 1–10.

[19] A. Srinivasan, W. Grutzeck, The adsorption of SO_2 by zeolites synthesized from fly ash, Environ. Sci. Technol. 33 (1999) 1464–1469.

[20] X. Querol, N. Moreno, J.C. Umana, R. Juan, S. Hernandez, C. Fernandez-Pereira, C. Ayora, M. Janssen, J. Garcia-Martinez, A. Linares-Solano, D. Cazorla-Amaros, Application of zeolitic material synthesized from fly ash to decontamination of waste water and flue gas, J. Chem. Technol. Biotechnol. 77 (2002) 292–298.

[21] N. Moreno, X. Querol, C. Ayora, C. Fernandez-Pereira, M. Janssen-Jurcovicova, Utilization of zeolites synthesized from coal ash for the purification of acid mine waters, Environ. Sci. Technol. 35 (2001) 3526–3534.

[22] W.U. Deyi, H.U. Zhanbo, X. Wang, H.E. Shengbing, H. Kong, Use of zeolitized coal fly ash in the simultaneous removal of ammonium and phosphate from aqueous solution, Front. Environ. Sci. Eng. China 1 (2) (2007) 213–220.

[23] S.S. Rayalu, A.K. Bansiwal, S.U. Meshram, N. Labhsetwar, S. Devotta, Fly ash based zeolite analogues: versatile materials for energy and environment conservation, Catal. Surv. Asia 10 (2006) 74–88.

[24] X.S. Zhao, G.Q. Lu, H.Y. Zhu, Effects of ageing and seeding on the formation of zeolite Y from coal fly ash, J. Porous Mater. 4 (1997) 245–251.

[25] K. Ojha, N.C. Pradhan, A.N. Samanta, Zeolite from fly ash: synthesis and characterization, Bull. Mater. Sci. 27 (6) (2004) 555–564.

[26] J. LaRosa, S. Kwan, M.W. Grutzeck, Zeolite formation in class F fly ash blended cement pasters, J. Am. Ceram. Soc. 75 (1992) 1574–1580.

[27] J. LaRosa, S. Kwan, M. Grutzeck, Self-generating zeolite cement composites, Mater. Res. Soc. Symp. Proc. 245 (1992) 211–216.

[28] M.W. Grutzeck, D.D. Siemer, Zeolites synthesized from class F fly ash and sodium aluminate slurry, J. Am. Ceram. Soc. 80 (1997) 2449–2453.

[29] M.W. Grutzeck, Zeolite synthesis from fly ash and cement kiln dust, in: Environmental Issues and Waste Management Technologies II, Ceramic Transactions, 1996, pp. 353–364.

[30] N. Shigemoto, H. Hayashi, K. Miyaura, Selective formation of Na-X zeolite from coal fly ash by fusion with sodium hydroxide prior to hydrothermal reaction, J. Mater. Sci. 28 (1993) 4781–4786.

[31] H.L. Chang, W.H. Shih, Conversion of fly ashes to zeolites for waste treatment, in: V. Jain, P. Palmer (Eds.), Environmental Issues and Waste Management Technologies, vol. 61, Ceramic Transactions, 1995, pp. 81–88.

[32] C.F. Lin, H.C. Hsi, Resource recovery of waste fly ash: synthesis of zeolite-like materials, Environ. Sci. Technol. 29 (1995) 1109–1117.

[33] M. Park, J. Choi, Synthesis of phillipsite from fly ash, Clay Sci. 9 (1995) 219–229.

[34] X. Querol, A. Alastuey, J.L. Fernandez-Turiel, A. Lopez-Soler, Synthesis of zeolites by alkaline activation of ferro-aluminous fly ash, Fuel 74 (1995) 1226–1231.

[35] N. Shigemoto, S. Sugiyama, H. Hayashi, K. Miyaura, Characteristics of Na-X, Na-A, and coal fly ash zeolites and their amorphous precursors by IR, MAS NMR and XPS, J. Mater. Sci. 30 (1995) 5777–5783.

[36] M. Qiu, C. Qian, J. Xu, J. Wu, G. Wang, Studies on the adsorption of dyes into clinoptilolite, Desalination 243 (2009) 286–292.

[37] S. Sohrabnezhad, A. Pourahmad, Comparison absorption of new methylene blue dye in zeolite and nanocrystal zeolite, Desalination 256 (2010) 84–89.

[38] S.K. Alpat, Ö. Özbayrak, Ş. Alpat, H. Akçay, The adsorption kinetics and removal of cationic dye, toluidine blue O, from aqueous solution with Turkish zeolite, J. Hazard. Mater. 151 (2008) 213–230.

[39] J. Yener, T. Kopac, G. Doğu, T. Doğu, Adsorption of basic yellow 28 from aqueous solutions with clinoptilolite and amberlite, J. Colloid Interface Sci. 294 (2006) 255–264.

[40] Y.B. Duygulu, Decolorization of Synthetic Dye Solutions by Using Basaltic Tephra and Clinoptılolite, MSc Thesis Graduate School of Natural and Applied Sciences, Middle East Technical Universıty, Turkey, 2004.

[41] B. Armağan, M. Turan, M.S. Çelik, Equilibrium studies on the adsorption of reactive azo dyes into zeolite, Desalination 170 (2004) 33–39.

[42] V. Meshko, L. Markovska, M. Mincheva, A.E. Rodrigues, Adsorption of basic dyes on granular activated carbon and natural zeolite, Water Res. 35 (2001) 3357–3366.

[43] G. Calzaferri, N. Gfeller, Thionine in the cage of zeolite L, J. Phys. Chem. 96 (1992) 3428–3435.

[44] V. Ramamurthy, D.R. Sanderson, D.E. Eaton, Control of dye assembly within zeolites: role of water, J. Am. Chem. Soc. 15 (1993) 10438–10439.

[45] M. Erol, A. Genç, M. Öveçoğlu, E. Yücelen, S. Küçükbayrak, Y. Taptık, Characterization of a glass–ceramic produced from thermal power plant fly ashes, J. Eur. Ceram. Soc. 20 (2000) 2209.

[46] F. Helfferich, Ion Exchange, Dover Publ., New York, USA, 1962.

[47] S. Paterson, The heating or cooling of a solid sphere in well stirred fluid, Proc. Phys. Soc. Lond. 59 (1947) 50–57.

[48] N. Kanan, M.M. Sundaram, Kinetics and mechanism of removal of methylene blue by adsorption on various carbons – a comperative study, Dyes Pigments 51 (2001) 25–40.

[49] M. Criado, A. Fernandez-Jimenez, A. Palomo, Alkali activation of fly ash: effect of the SiO_2/Na_2O ratio part I: FTIR study, Micropor. Mesopor. Mater. 106 (2007) 180–191.

[50] Y. Ding, Z. Chen, J. Xie, R. Guoi, Comparative studies on adsorption behavior of thionine on gold nanoparticles with different sizes, J. Colloid Interface Sci. 327 (2008) 243–250.

[51] M.S. Plesset, F. Helfferich, J.N. Franklin, Ion exchange kinetics. A nonlinear diffusion problem. II. Controlled exchange of univalent and bivalent ions, J. Chem. Phys. 29 (1958) 1064–1069.

[52] A.C. Wahl, N.A. Bonner, Radioactivity Applied to Chemistry, John Wiley and Sons, Inc., New York, 1958.

[53] T.C. Huang, F.N. Tsai, Kinetic studies on the isotopic exchange of calcium ion and calcium carbonate, J. Inorg. Nucl. Chem. 32 (1970) 17–31.
[54] R. Han, J. Zhang, P. Han, Y. Wang, Z. Zhao, M. Tang, Study of equilibrium, kinetic and thermodynamic parameters about methylene blue adsorption onto natural zeolite, Chem. Eng. J. 145 (2009) 496–504.
[55] H. Freundlich, Über die adsorption in lösungen, Z. Phys. Chem. 57 (1907) 385–470.
[56] R. Atkin, V.S.J. Craig, E.J. Wanless, S. Biggs, Mechanism of cationic surfactant adsorption at the solid aqueous interface, Adv. Colloid Interface Sci. 103 (2003) 219–304.